Initiation and resolution of interhomolog connections: crossover and non-crossover sites along mouse synaptonemal complexes

Peter B. Moens*, Edyta Marcon, Joel S. Shore, Nazafarin Kochakpour and Barbara Spyropoulos

Department of Biology, York University, Toronto, Ontario, M3J 1P3, Canada

*Author for correspondence (e-mail: moens@yorku.ca)

Accepted 8 January 2007
Journal of Cell Science 120, 1017-1027 Published by The Company of Biologists 2007
doi:10.1242/jcs.03394

Summary

Programmed double-strand breaks at prophase of meiosis acquire immunologically detectable RAD51-DMC1 foci or early nodules (ENs) that are associated with developing chromosome core segments; each focus is surrounded by a γH2AX-modified chromosome domain. The 250-300 ENs per nucleus decline in numbers during the development of full-length cores and the remaining foci are relatively evenly distributed along the mature cores (gamma distribution of ν=2.97). The ENs become transformed nodules (TNs) by the acquisition of RPA, BLM, MSH4 and topoisomerases that function in repair and Holliday junction resolution. At the leptotene-zygotene transition, TNs orient to positions between the aligned cores where they initiate structural interhomolog contacts prior to synaptonemal complex (SC) formation, possibly future crossover sites. Subsequently, TNs are associated with SC extension at the synaptic forks. Dephosphorylation of TN-associated histone γH2AX chromatin suggests annealing of single strands or repair of double-strand breaks DSBs at this time. Some 200 TNs per pachytene nucleus are distributed proportional to SC length and are evenly distributed along the SCs (ν=~4). At this stage, γH2AX-modified chromatin domains are associated with transcriptionally silenced sex chromosomes and autosomal sites. Immunogold electron microscope evidence shows that one or two TNs of the 10-15 TNs per SC acquire MLH1 protein, the hallmark of reciprocal recombination, whereas the TNs that do not acquire MLH1 protein relocate from their positions along the midline of the SCs to the periphery of the SCs. Relocation of TNs may be associated with the conversion of potential crossovers into non-crossovers.

Supplementary material available online at
http://jcs.biologists.org/cgi/content/full/120/6/1017/DC1

Key words: Chiasmata, Interference, DMC1, RPA, MLH1, γH2AX, Recombination nodules, Synaptonemal complex, Mouse meiosis

Introduction

During prophase of meiosis, homologous chromosomes undergo synapsis, genetic exchange (recombination/crossing-over) and gene conversion. Many of these activities are associated with the cores of meiotic chromosomes and with synaptonemal complexes when present.

Prominent among the tools for the recognition of in situ mouse meiotic prophase chromosome events are antibodies to meiotic chromosome core components SYCP3, to cohesins SMC1β, SMC3 and STAG3 and REC8, to transverse filaments SYCP1 (Dobson et al., 1994; Revenkova and Jessberger, 2005), and to chromatin modifications by phosphorylation of histone H2AX (Fernandez-Capetillo et al., 2004; Turner et al., 2005). Recombination events have been tracked with antibodies against RAD51 and DMC1 (homologs of *E. coli* RecA) (Tarsounas et al., 1999), to single-strand binding protein RPA, to the RecQ helicase chromosome-stability protein BLM, to the MSH4 homolog of *E. coli* MutS, and to the crossover-associated proteins MLH1 and MLH3, homologs of *E. coli* DNA-repair protein MutL. We have used these tools to show that most of the chromosome-core-associated early RAD51-DMC1 complexes – termed early nodules (ENs) – acquire RPA, BLM and MSH4 protein, whereas the RAD51-DMC1 component is lost from such transformed nodules (TNs; Fig. 1) (Moens et al., 2002).

Here, we consider the functional implications of EN and TN localization, time course and dynamics in relation to reciprocal recombination – MLH1-defined recombination nodules (RNs) – and to non-crossovers. RNs correlate in number and position with reciprocal genetic recombination in *Drosophila melanogaster* (Carpenter, 1975; Carpenter, 1979a; Carpenter, 1979b) and they mark the positions of chiasmata along mouse pachytene synaptonemal complexes (SCs) (Marcon and Moens, 2003). Using fluorescence in situ hybridization (FISH) painting of individual mouse chromosomes at meiotic prophase, the positions of MLH1-defined RNs have been enumerated for each chromosome in a large sample of meiotic prophase nuclei (Froenicke et al., 2002). The technique takes its strength from its simplicity and positional accuracy. Furthermore, this methodology is independent of inheritance constrains such as the viability of germ cells, gametes or zygotes.

Our results on the elimination of excess potential crossovers share features of the interference models of Egel (Egel, 1978; Egel, 1995), King and Mortimer (King and Mortimer, 1990) and Gilbertson and Stahl (Gilbertson and Stahl, 1996). Our observations on the initiation and resolution of recombinational events may account for the early prophase regulation of crossovers and non-crossovers in *Arabidopsis thaliana* (Higgins et al., 2005) and in mice (de Boer et al., 2006).

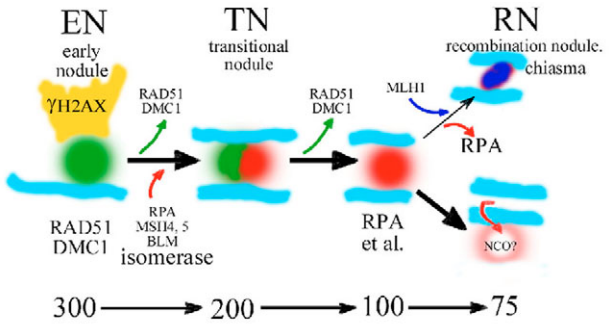

Fig. 1. Development of meiotic chromosome core-associated recombination protein complexes in mouse spermatocytes [adapted from Moens et al. (Moens et al., 2002)]. About 250 to 300 ENs (green), become associated with the chromosome cores (blue) prior to synapsis. They are spherical structures, about 100 nm in diameter, and are identified by antibodies to RAD51 and DMC1 protein (green). They are the sites of programmed, double-strand DNA breaks at meiotic prophase and they are associated with phosphorylated histone H2AX (yellow; this report). The ENs are transformed into ~200 synaptonemal complex (SC)-associated, RPA-defined TNs (SCs, parallel blue lines; TN, red) by the acquisition of several proteins – RPA, BLM, MSH4, MSH5 and topoisomerases – while they loose the RAD51-DMC1 and γH2AX components. In the mouse spermatocyte nucleus, about 25 of the TNs acquire MLH1 protein (blue) that mark the sites of chiasmata. The remaining TNs are resolved as non-crossovers and they relocate to the outside the SCs (this report).

Results

Initiation of RAD51-DMC1 EN sites

Numbers and distribution of double-strand breaks (DSBs), as revealed by RAD51-DMC1 ENs, are regulated such that there are maximally between 250 to 300 foci per mouse spermatocyte nucleus. The first appearance of ENs (Fig. 2A, 100 red foci) is associated with chromatin modification by phosphorylation of histone H2AX (Fig. 2A, diffuse red areas) and by the formation of short chromosome core segments (Fig. 2A, short green structures). Most of the ENs (Fig. 2A, red foci) are connected to short core segments and the excess of core segments over ENs suggests that the segments form in advance of ENs. γH2AX chromatin domains and ENs appear to coincide, suggesting that they develop simultaneously. At a somewhat later leptotene stage, the γH2AX chromatin domains are organized in EN-associated flares (Fig. 2B) and, when core formation is extensive, the ENs and γH2AX domains become aligned (Fig. 2C).

Since ENs are the precursors of RPA-defined TNs (RPA-TNs), we examined the distribution of ENs along cores prior to pairing to determine the correlation between EN and TN distribution. In zygotene nuclei, chromosomes are only partially synapsed (Fig. 2D,E). We measured distances between 100 ENs along unpaired cores of three zygotene nuclei. The shape of the gamma distribution (ν=2.97) suggests that the foci are relatively evenly rather than randomly distributed along the unpaired cores (supplementary material Fig. S1A,B). We conducted a simulation to explore the effect of synapsis for two homologous cores each with 500 foci and a shape parameter ν=2.97. We then estimated the resulting shape for the 1,000 data points along the SC formed by the

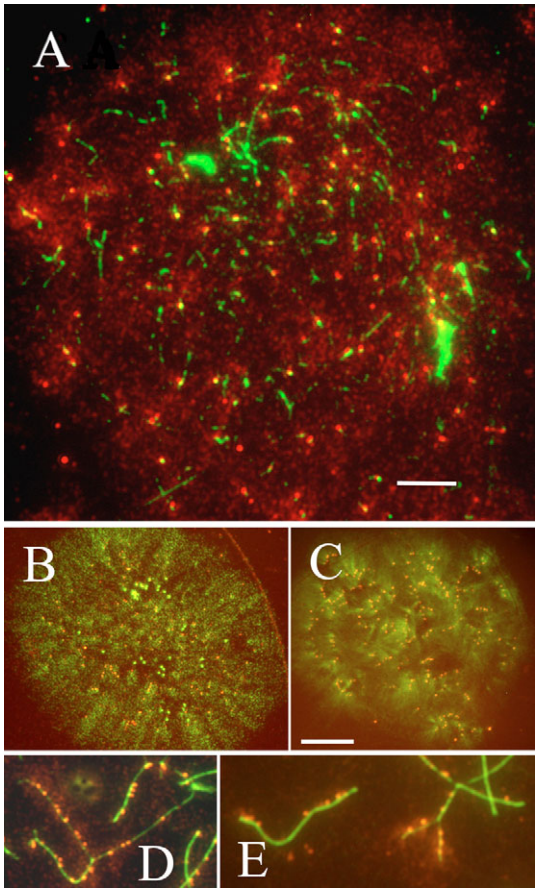

Fig. 2. Development of nodules from leptotene into zygotene. (A) An early leptotene spermatocyte nucleus with the stage defined by the earliest formation of SYCP3 chromosome-core segments (FITC, green). By the internal clock of the progression from zero to 250-plus RAD51-DMC1 foci (Rhodamine, red foci), this nucleus with 100 foci is still developing RAD51-DMC1 sites. The foci are usually connected to a core segment and they are the centres of diffuse γH2AX domains (Rhodamine, red). (B) Reorganization of γH2AX domains (FITC, green). At a slightly later leptotene stage, the spherical domains rearrange into flare-shaped domains. (C) Alignment of 230 foci and associated γH2AX flares (FITC, green). (D,E) Zygotene chromosome cores. Foci of the unpaired cores and recently paired cores (green) are associated with γH2AX (Rhodamine, red domains) but the foci of fully synapsed cores have no, or strongly reduced, γH2AX domains. Presumably annealing and/or repair has been completed.

synapsed cores as ν=1.65±0.33 (± s.e.m.), different from a random gamma distribution with shape ν=1 (G_{df1}=131.5, P<0.001) (supplementary material Fig. S1C,D). Thus theoretically, synapsis reduces the level of even distribution from 2.97 to 1.65.

To test the possibility that γH2AX is involved in regulation of the numbers and distribution of ENs, we measured distances between TNs in *H2ax*$^{-/-}$ pachytene spermatocytes. The gamma distribution of distances (ν=2.3±0.27; supplementary material Fig. S4) suggests that in the absence of chromatin modification, TN spacing is still fairly even but low numbers of foci and synaptic defects limit the interpretation of the results.

Initial contacts between aligned cores have RPA-defined TNs

Initiation of close connections between aligned chromosome cores is shown in Fig. 3 with immunofluorescence of the chromosome cores and centromeres (core, cen; FITC, green), TN foci (RPA-TNs; Rhodamine, red) and SCs (anti-transverse filament protein SYCP1; Rhodamine, red, or yellow-to-orange where the fluorochromes FITC and Rhodamine overlap). The spermatocyte nucleus shown in Fig. 3 is in transition from a late leptotene to early zygotene stage with broadly aligned chromosome cores, a few closely aligned segments, and sporadic SC segments. These features are common to the 40 digitally recorded fluorescent images of spermatocyte nuclei at the transition from leptotene to the zygotene stage of meiotic prophase nuclei.

At early meiotic prophase, RPA-defined TNs are associated with the chromosome cores (Fig. 3, carets). Bivalent #2 in Fig. 3 demonstrates the critical event: that the initial point of close contact between aligned cores is associated with an RPA-TN. The same position of the RPA-TN between the closely aligned cores is evident in bivalent #1. Bivalent #1 furthermore demonstrates that a core-associated RPA-TN (*) can establish an interhomolog connection at a distance, as witnessed by the inflection (i) in the opposite chromosome core.

There is no SC formation in bivalents #1, 2 or 3 judging by the absence of SYCP1 (transverse filament) staining. Thus, the initial close contacts between aligned cores appear to involve the RAD51-DMC1-RPA complex and appear to precede central-element formation. Apparently, even fairly extensive close alignment in bivalent #3 precedes SC formation. This phenomenon is also seen in most of #4 but it has initiated distal SC formation. Close alignment of cores without SYCP1 protein was not anticipated. The RPA-TN foci at the inflections of bivalents #1, 2 and 3 appear to be the brightest foci, possibly indicating the most abundant protein complexes.

Initial distal RPA-TN interhomolog contacts correlate with MLH1 positions

At the leptotene-zygotene transition, RPA-TN-mediated close alignment of cores initiate preferentially at the distal parts of the cores (Fig. 3, pair #1 and #2) and, at late zygotene, the proximal segments (centromeres) tend to be the last to synapse (Fig. 4A). In general, we observed distal preference in 21 nuclei at the onset of close alignment, in 11 nuclei with

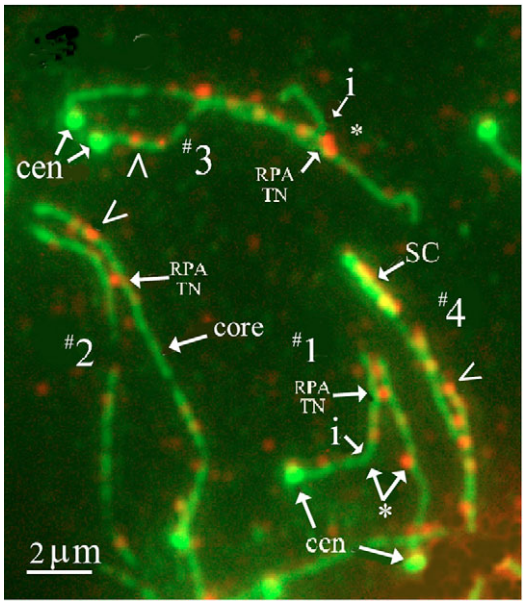

Fig. 3. An early prophase spermatocyte nucleus where inter-homolog connections are established in the context of RPA-TN foci prior to SC formation [RPA-TN foci, red; SCYP1 cores and centromeres (cen), FITC, green]. Bivalent #2 has broadly aligned cores with one RPA-TN focus at the site of close alignment prior to SC formation. Other TNs are associated with the unpaired cores (caret). Bivalent #1 has two TNs at the distal, closely aligned cores and an additional RPA-TN interhomolog connection at the inflection (i, asterisk). Bivalent #3 has RPA-TN foci along and at both ends of a long closely aligned segment. Close alignment is extensive in bivalent #4 and SC formation (SC) has been initiated in the distal segment.

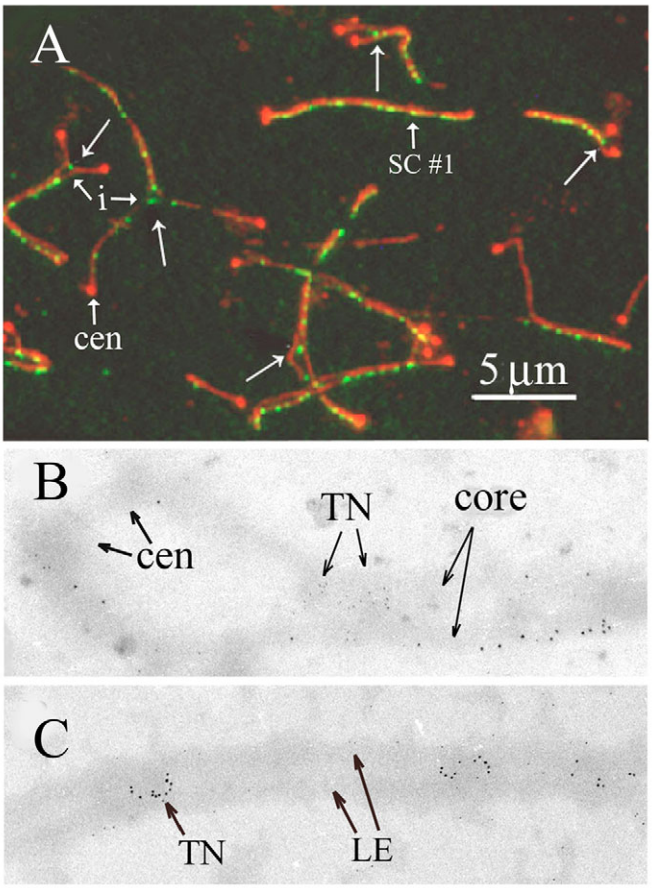

Fig. 4. Progression of SC formation (SC; red). (A) Synaptic forks at the points of synaptic progress are associated with TNs (green foci, arrows). The inflections (i) suggest a structural connection between the two homologs at the site of the TN. At later prophase, the chromosomes are completely synapsed and the SCs can have 10 or more TNs each (SC #1). The centromeres (cen; red) are frequently the last to pair. (B) Immunogold-defined positions of TNs at zygotene. The synaptic fork has two TNs labelled with 5-nm gold particles. The lateral elements (LEs) are labelled with 10-nm gold particles. (C) A mature pachytene SC with lateral elements and medially located TNs (10-nm gold). The width of the SC is approximately 250 nm.

Table 1. MLH1 positions relative to SC ends

Cell number	Distance measured		χ^2	SCs
	Cen to MLH1	MLH1 to end		
01	200	95	36	18
02	112	48	26	13
09	146	56	40	16
11	176	65	52	16
16	211	56	90	12
17	117	61	18	13
Total	662	381	262	88

Total χ^2 (1:1)=3.3 d.f.=1 P<0.005

Cen, centromere; d.f., degrees of freedom.

synapsis in progress, and in 10 nuclei near the completion of synapsis. Eventually, TNs are distributed along the length of the bivalent (Fig. 3, Fig. 4, Fig. 5A) but crossover-related MLH1 foci tend to occur distally (Froenicke et al., 2002; de Boer et al., 2006). If initial distal RPA-TN close contacts are related to MLH1 foci, it can be expected that the positions of the two types of foci will be correlated. To verify that, in our samples, the initial distal TN positions correlate with distal MLH1 foci, we measured the positions of MLH1 foci relative to either end of the SC in six nuclei (Table 1). As expected, the MLH1 foci are, on average, significantly closer to the distal end than to the proximal ends of autosomal SCs with a single MLH1 focus (P<0.005). Thus, the distal positions of initial TN contacts correlate with the distal RN positions, and, conversely, the positions of the proximal TNs correlate only weakly with RN positions. In the context of early crossover versus non-crossover decisions, the proximal TNs have a low probability of becoming crossovers.

Synaptonemal complex extension

At zygotene, the synaptic stage of meiotic prophase, transverse filaments (SYCP1) bring the cores into a continuous parallel alignment in a zipper-like manner. The zygotene nucleus in Fig. 4A (SCs, red; TNs, green) presents evidence that TNs are regularly associated with the progression of synapsis. At each of five synaptic forks in Fig. 4A, there is a TN at the synaptic fork (long arrows). It is evident from the inflection of the cores at 'i' that the RPA-TN between the cores is connected to both cores, indicative of a structural inter-homolog interaction. Fig. 4A further demonstrates that, at late zygotene, the proximal centromeric ends (cen) are often the last to synapse. When the cores are fully synapsed, there is a fairly dense array of TN foci along the entire SC (Fig. 4A, SC #1; Fig. 5A). During subsequent development, the numbers of TNs decline (Fig. 5B).

Positions of TNs can be identified at electron microscopic resolution with immunogold labelling (Fig. 4B,C). There is one TN (5-nm gold) at the synaptic fork and one next to it where the cores/lateral elements (10-nm gold) are in close alignment (Fig. 4B). The width between the cores suggests that no central element has formed as yet. The TNs of the mature SC in Fig. 4C (TN, 10 nm gold) are positioned along the midline of the SC between the lateral elements.

There are a limited number of TNs along each of the SCs (Fig. 4A) and it would therefore seem that the TNs mediate interhomolog connections in an intermittent pattern as in the manner of a garment closure by buttons. Subsequently, transverse filament-mediated zippering establishes the continuous parallel alignment of the lateral elements. The numbers of TN 'buttons' along each SC is greater by an order of magnitude than the eventual numbers of reciprocal crossovers and it follows that most of these interactions will not give rise to reciprocal crossovers.

MLH1 foci without SCs

Fig. 3 demonstrates that RPA-TN foci can be present between closely aligned cores in the absence of an SC structure as defined by SYCP1 transverse filaments. In *Sycp3*$^{-/-}$ oocytes, SC formation is incomplete (Yuan et al., 2000) but the cores and SC-like structures in oocytes have their normal allotment of TNs, some 250 core-associated foci (Fig. 6A, red foci) and

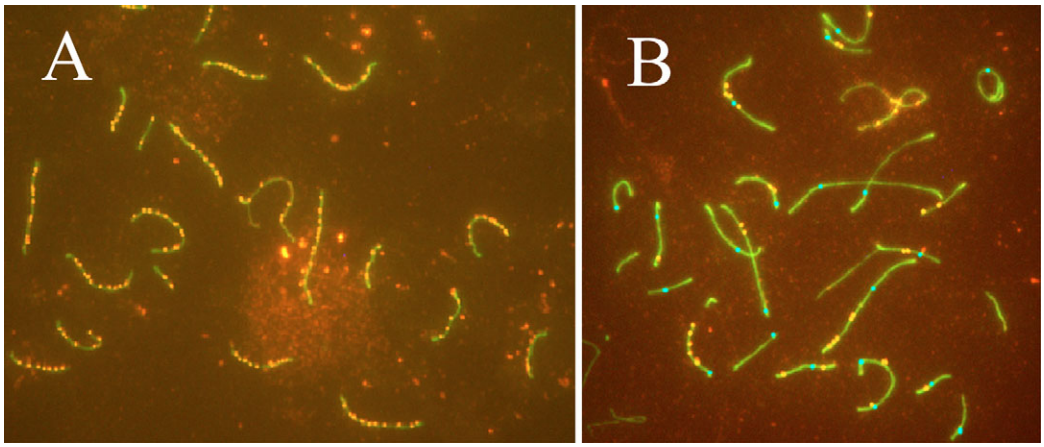

Fig. 5. Number and distribution of TNs. (A) A mid-pachytene nucleus with 140 RPA-TN foci (Rhodamine, red, but yellow on a green background) positioned fairly evenly along the SCs (green) (see supplementary material Fig. S4, cell 02). The number of TNs in this nucleus has declined from the original 250+ foci at zygotene. (B) At late pachytene, there remain few TNs – 33 in this nucleus (see supplementary material Fig. S5, cell 09). Uneven loss of TNs leaves an uneven distribution along the SCs and some SCs have no TNs. MLH1 foci (blue) have developed by this stage.

150 SC-associated foci (Fig. 6A, yellow foci), a total of 400 foci in Fig. 6A [oocytes have more foci than spermatocytes (Kolas et al., 2005)]. Because SC formation is incomplete, many of the TNs remain associated with unpaired cores and will not form an SC. If a non-SC, RPA-TN interhomolog connection develops into an MLH1-defined RN, it can be expected to appear independent of SYCP1 at a later prophase stage. The three cells in Fig. 6B-D are from a single ovary of a 17.5 days post coitus *Sycp3*$^{-/-}$ foetus. They are all in mid to late pachytene, judging by the foetal age and the numerous MLH1 foci that first appear at mid pachytene (Kolas et al., 2005). The different lengths of the SC segments (anti-SYCP1, bright red, Rhodamine) reflect levels of defective synapsis, most severe in Fig. 6B, intermediate in Fig. 6C and minimal in Fig. 6D. The arrows mark some of the MLH1 foci (FITC, green) that are associated with cores (anti-SMC3, weak Rhodamine staining) but not with SYCP1-defined SCs. In oocytes of the type shown in Fig. 7B, 30% of the MLH1 foci are SYCP1 independent (n=50); in oocytes of the type illustrated in Fig. 6C, that number is 16% (n=55); in oocytes of the type appearing in Fig. 7D, it is 3% (n=114); and in two oocytes with long SCs, there were no SYCP1-independent MLH1 foci. These observations indicate that SYCP1 transverse filaments are not a necessary requirement for the development of MLH1-defined RNs.

Distribution of RPA-TN foci

For early- to mid-pachytene nuclei with between 200 and 150 SC-associated TNs, the number of RPA-TNs per unit length of SC is relatively constant for different length SCs: about 1 TN per 1 μm SC (Fig. 5A). Statistical analysis of measured distances between 215 autosomal TNs fitted to a gamma distribution yields a shape parameter of 4.2 with confidence intervals of 2.6 to 6.1, indicating that the shape differs from 1 and implies a non-random distribution (supplementary material Fig. S2 for cell 08). The same analysis of the more

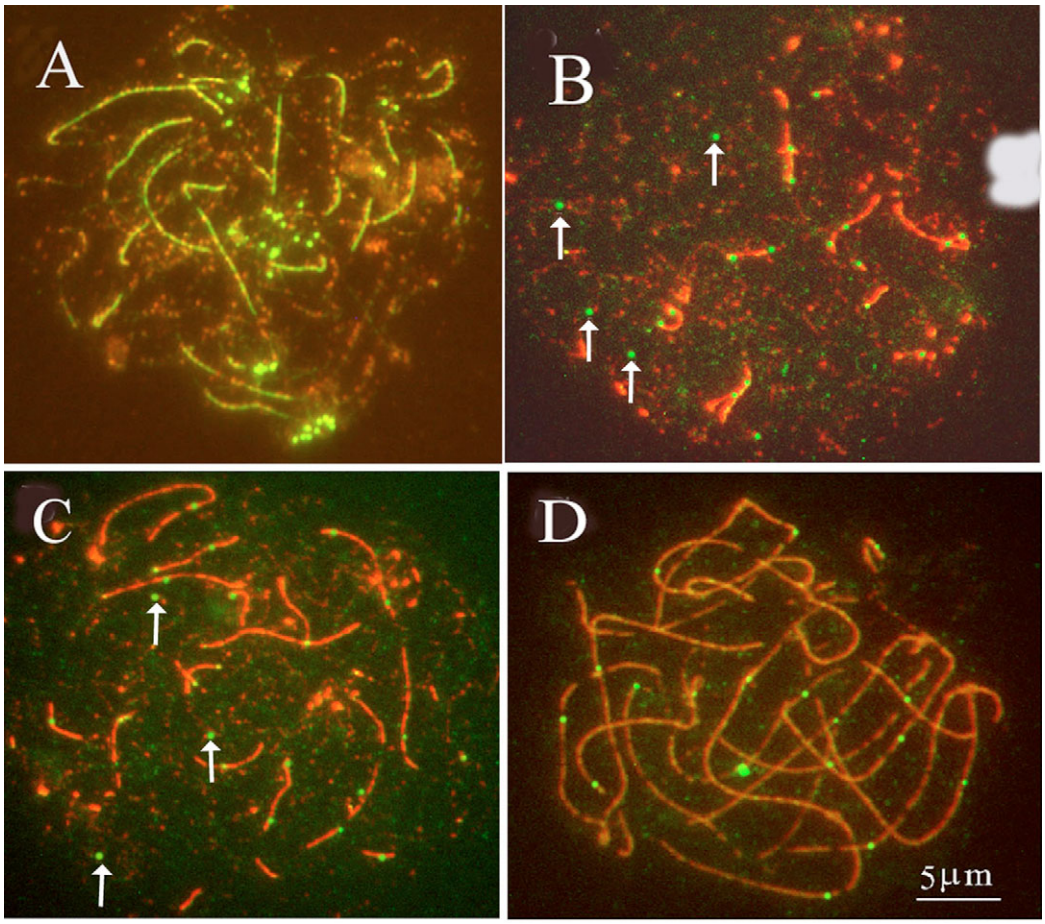

Fig. 6. TNs and MLH1 foci in *Sycp3*$^{-/-}$ oocytes. (A) An early prophase nucleus from a 15.5-day old foetus with 150 TNs (yellow) associated with SC-like structures (bright green) and 250 TNs (red) associated with unpaired cores (weak green). Immunostaining of RPA-TNs: core components SMC3, SYCP1, Rhodamine, red; centromeres, FITC, green. (B-D) Three pachytene oocytes nuclei from one ovary of a 17.5-day old foetus with different levels of synaptic defects. Chromosome cores were immunostained with rabbit anti-SMC3 (Rhodamine, weak red) and SC central elements with rabbit anti-SYCP1 (Rhodamine, bright red). The MLH1 foci are visualized by mouse anti-MLH1 and FITC-conjugated secondary antibody (green). (B) An oocyte nucleus with severe synaptic defects. Arrows mark some of the MLH1 foci that are not associated with brightly stained SYCP1 segments. (C) An oocyte nucleus with intermediate synaptic defects. There are more and longer SYCP1 segments and fewer free MLH1 foci (arrows). (D) A near-normal looking oocyte nucleus with well-developed SYCP1-defined SCs, few unsynapsed cores, and no free MLH1 foci.

advanced cell 02 with 140 inter-TN distances has a shape parameter of 3.8 (supplementary material Fig. S3). When there are fewer TN foci at later prophase (Fig. 5B, cell 09, 33 foci), the distances between foci are more irregular, resulting in a shape parameter of the distances between TNs of 1.2 with 95% confidence intervals of 0.5 and 1.9 that suggest no significant deviation from a random distribution (supplementary material Fig. S5, cell 09). A combination of five nuclei with between 43 and 27 foci similarly fits a gamma distribution with a shape of 1 (supplementary material Fig. S5) indicative of a random distribution. Apparently, the removal of TNs does not follow a predictable pattern. Thus, the non-random distribution of TNs at early pachytene is no longer evident at late pachytene.

High resolution of TN distribution along the SCs can be assessed by enumeration of sequential 1-μm SC segments that contained zero, one, or more immunogold-defined RPA foci in 42,000× magnification electron micrographs of full-length SCs. Data from four full-length SCs in one nucleus and six SCs in a second nucleus that are in the early stages of RN formation (late pachytene, few foci, bracketed segment in Fig. 7E) are shown in Table 2. Asterisks mark the SCs that have an RN containing RPA and MLH1 antigen. A sample SC with eight TNs and one MLH1 focus is shown in Fig. 7A. The comparison of observed and expected distribution of TNs, in Table 2, does not show significant deviation from a random Poisson distribution (P=0.5). Apparently, as shown above for the nucleus in Fig. 5B, when few TNs remain at late pachytene, they tend to have a random distribution along the SCs (supplementary material Fig. S5). The loss of TNs is not in concert among the SCs – some have lost all TNs whereas others still have several TNs (Fig. 5B).

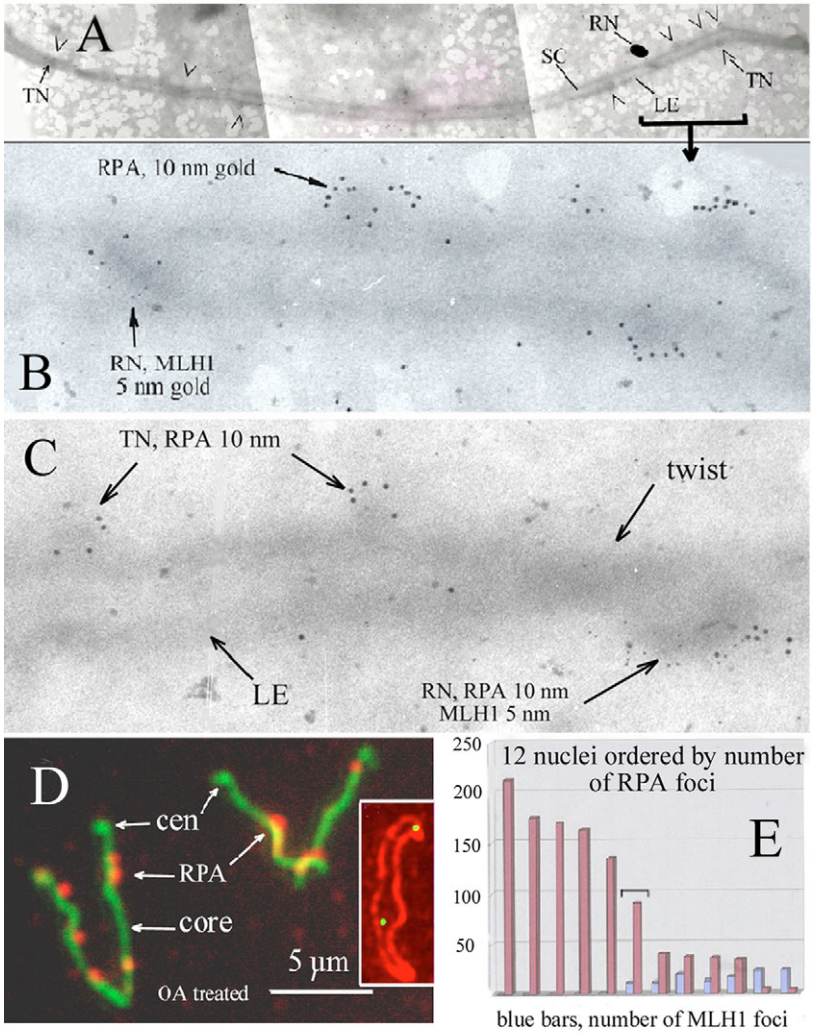

Fig. 7. RPA-TN and MLH1 dynamics. (A) A full-length pachytene SC with eight RPA-TN foci (TN, carets) and one recombination nodule (RN, elliptical bullet). (B) High resolution of the bracketed segment in A. The 10-nm gold grains mark the positions of RPA protein and the 5-nm particles that of the MLH1 protein. Colocation of 10-nm and 5-nm gold grains at the RN suggests that the RN is derived from a TN. Other TNs have relocated from their positions between the lateral elements of the SC to the periphery of the lateral elements. (C) Same as B but the twist in the SC shows that the RN is on the surface of the SC. (D) Okadaic acid treatment of spermatocytes causes premature separation of the lateral elements (FITC, green). The TNs are no longer between the cores but are associated with the cores. Inset: RNs (green foci), by contrast, remain between the separated lateral elements (red) at the positions of the chiasmata. (E) Summary of RPA-TN and MLH1-RN dynamics for 12 mouse spermatocyte nuclei. MLH1 foci appear when the number of TNs has been reduced to about 100 foci per nucleus. Image in A and data for Table 2 were derived from SCs in the bracketed portion of the graph.

Do TNs become RNs?

Approximately 200 RPA-containing recombination complexes are associated with the full-length SCs of pachytene nuclei prior to the appearance of MLH1 foci (Fig. 5A, Fig. 7E). The numbers decline to zero at the end of meiotic prophase. MLH1 foci appear when the number of TNs has declined to about 100 (Fig. 7E). As the TNs decline in number, the number of MLH1 foci increases to about 25 per nucleus. If a subset of RPA-TNs gives rise to RNs, we expect to find that MLH1 protein becomes associated with RPA-defined TNs. To test that assumption, we focus on the narrow window (Fig. 7E, bracket) where TNs are still relatively abundant at the time when MLH1 foci are just appearing (Fig. 7E) as judged by the fact that not all SCs of a given nucleus have as yet acquired an MLH1 focus. Fig. 7B,C illustrates that the RPA protein (10-nm gold particles) is present in the RN as defined by the 5-nm gold particles that recognize MLH1 protein. In Fig. 7B, the RN has five 5-nm gold grains (MLH1) and four 10-nm gold grains (RPA). In Fig. 7C, the ratio is 12:6. The same colocation of MLH1 and RPA was observed in the seven SCs with an RN (Table 2). Because both RPA and MLH1 are present in the newly formed RNs, it would appear that RNs are a subset of the preceding RPA-containing TNs. It is a specific subset in the sense that, in the male, there are commonly only one or two RN-MLH1 sites per SC versus the 10 to 15 TN sites per SC.

Table 2. Random positions of late TNs along individual SCs

SC	Numbers of TNs per segment					No. of 1-μm samples	No. of foci
	0	1	2	3	4		
1	1	2	2	0	0	5	6
2*	7	3	0	0	1	11	7
3*	5	2	1	0	0	8	4
4*	1	3	1	0	0	5	5
5	4	1	2	0	0	7	5
6*	3	3	2	0	0	8	7
7*	6	2	0	0	0	8	2
8	6	3	0	1	0	10	6
9*	7	2	2	0	0	11	6
10*	5	2	3	1	0	11	11
Obs	45	23	13	2	1	84	59
Exp	41.6	29.2	10.3	2.4	0.4		
χ^2	0.28	1.32	0.70	0.10	0.90		

Total χ^2=3.3 d.f.=3 P=0.37

*, SCs having an RN; Obs, observed; Exp, expected; d.f., degrees of freedom.

Resolution of TN interhomolog interactions

Immunofluorescence and electron microscope immunogold examinations of TN dynamics suggest a possible mechanism of TN elimination. While close contacts and SCs develop, the TNs are located between the lateral elements (Figs 3, 4). Later, during the pachytene stage, the TNs that do not acquire MLH1 protein relocate from the central element to the outer edges of the lateral elements (Fig. 7A-C). The TN relocation in Fig. 7B,C is in a late prophase nucleus where one or more SCs have acquired MLH1-defined RNs while there are still RPA foci (Fig. 7E, bracketed region). TN relocation from the central element of the SC to the lateral elements can be further detected by culturing spermatocytes briefly (1-2 hours) in the presence of the phosphatase inhibitor okadaic acid that prematurely separates the lateral elements. Evidence from treated cells indicates that at advanced prophase, the TNs (Fig. 7D, anti-RPA, Rhodamine, red) are physically associated with the lateral elements (anti-SYCP3, FITC, green) rather than with the region between the lateral elements. The inset in Fig. 7D shows that, under these same conditions, RNs (anti-MLH1, FITC, green) remain associated with a chiasma between the lateral elements (anti-SYCP3, Rhodamine, red) (Marcon and Moens, 2003). In summary, TNs that are first associated with cores, relocate to between the lateral elements and display interhomolog connections. Subsequently, some acquire MLH1 protein; the rest relocate from the medial region of the SC to the lateral elements and are eliminated (Fig. 1).

γH2AX chromatin modification at ENs and TNs

Histone H2AX of large chromatin domains (2+ megabases) at the sites of DSBs becomes phosphorylated (Fernandez-Capetillo et al., 2004). At meiosis, the sites of DSBs can be detected by immunocytology of RAD51 and DMC1 proteins, components of ENs and the associated histone γH2AX (Fig. 2). Phosphorylation takes place at early leptotene (Fig. 2A,B) before the ENs/TNs become aligned (Fig. 2C). It is expected that phosphorylation levels decline as annealing of single strands and repair take place at the sites of DSBs. Fig. 2D,E and Fig. 8A illustrate the presence of γH2AX at ENs/TNs along the unpaired cores of a partially synapsed bivalent while the synapsed part of the same bivalent has little or no γH2AX associated with the TNs. The nearby bivalents have completed synapsis and the ENs/TNs are no longer associated with γH2AX domains. It is concluded that DSB are no longer detected as breaks by the cell when synapsis takes place.

At a later stage (Fig. 8B,C), the X-Y chromatin is the major γH2AX domain in the nucleus. γH2AX has been reported to function in the transcriptional silencing of the X and Y chromatin (Turner et al., 2005). We observe that, in addition, there are autosomal γH2AX

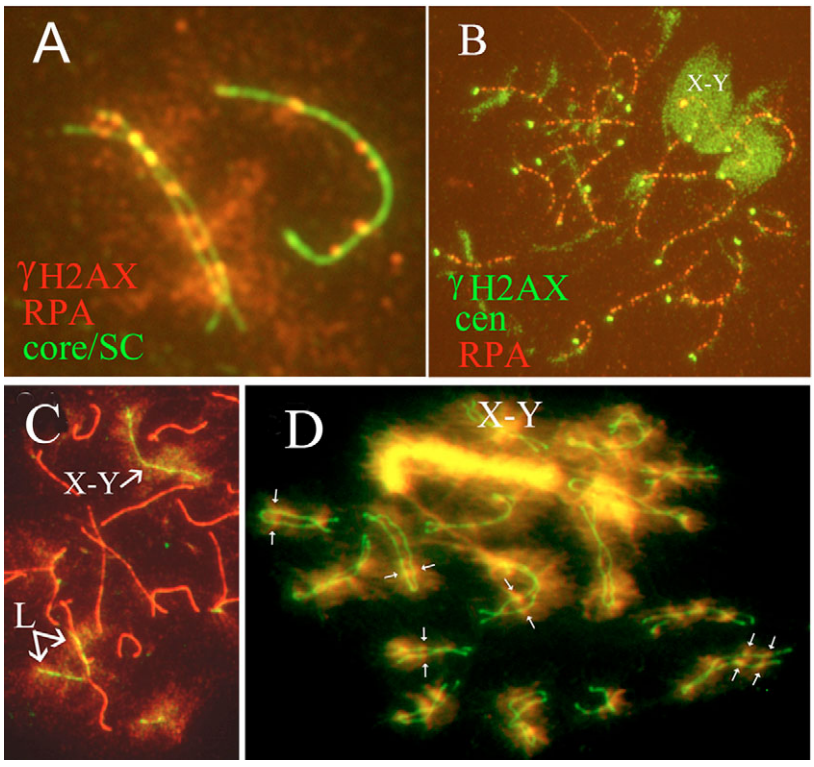

Fig. 8. γH2AX is associated with DSB of ENs and transcriptional silencing. (A) γH2AX domains (red) are associated with the foci (yellow) before synapsis and, when the cores synapse to form an SC (green), the γH2AX domains are minimal, which is possibly an indication that DSBs are no longer detectable. (B) At pachytene, histone H2AX of the X-Y sex chromatin is transcriptionally silenced by phosphorylation (FITC, green). As well, there are autosomal γH2AX domains (FITC, green) that do not appear to be associated with TNs (red foci) and may represent transcriptional silencing of autosomal loci. (C) γH2AX chromatin modification of the sex body and laggards (L). A further indication that pachytene chromatin modification (yellow) may be unrelated to DSBs. Typically, cores (red) that fail to synapse (laggards, L), acquire γH2AX domains in association with ATR and TOPBP1 on the unpaired cores. (D) In prematurely separated lateral elements (green) caused by okadaic acid treatment, some of the γH2AX domains (yellow) are paired (matched arrows), suggesting silencing of autosomal sites.

domains (Fig. 8B) that are not necessarily located at TNs and those may be sites of autosomal transcriptional silencing rather than sites of unrepaired breaks. TN-independent γH2AX domains can also be seen at stretches of synaptic failures (Fig. 8C; L, laggard). At the laggards, γH2AX chromatin is associated with ATR (ataxia telangiectasia- and RAD3-related) and TOPBP1 (topoisomerase binding protein) at the cores rather than at the TNs.

If late γH2AX chromatin is involved in silencing, then both alleles of a given gene should be silenced. With the phosphatase inhibitor, okadaic acid, the cores of an SC can be separated prematurely and, in such preparations, paired γH2AX sites are fairly common (Fig. 8D, arrows) suggesting that indeed silencing of autosomal foci rather than DSB repair may account for autosomal γH2AX chromatin domains at later pachytene stages. In these preparations, the removal of TN-associated γH2AX is restricted due to the presence of the phosphatase inhibitor.

The effect of γH2AX chromatin modification on DSB and TN distribution was assessed in spermatocytes deficient for histone H2AX (Celeste et al., 2002). There appeared to be fewer TNs but the 140 measured inter-TN distances showed an even distribution (gamma 2.3) (supplementary material Fig. S4).

Discussion

The numbers and positions of RAD51-DMC1 recombination complexes as indicators of programmed double-strand breaks (DSB) at prophase of meiosis (Shinohara et al., 2000; Blat et al., 2002) occur in a highly regulated pattern. The wild-type yeast genome acquires some 64 breaks (Bishop, 1994); the mouse genome has 250-300 DSBs in the male and about 500 in the female (Ashley et al., 1995; Moens et al., 1997; Moens et al., 2002; Kolas et al., 2005); and the Easter lily genome collects some 2,000 DSBs (Anderson et al., 1997). In yeast and mouse, recombination-related immunofluorescent foci are distributed proportionally to synaptonemal complexes lengths (Fig. 6A, supplementary material Fig. S2C,D) (Fung et al., 2004; de Boer et al., 2006). Some of the foci become crossovers with the classic pattern of genetic interference such that the probability of a second crossover is a function of the distance from the first site (Jones, 1984; Jones, 1987; Froenicke et al., 2002). In spite of the large differences in species-specific numbers of recombination-related foci, the final numbers of crossovers are quite similar, between 20 and 50 for mouse and lily. By observing the development and demise of recombination complexes in wild-type and mutant mouse spermatocytes, we expect to gain insight into the manner by which numbers and distribution are regulated.

RAD51-DMC1 foci, numbers and distribution

The first RAD51-DMC1 immunofluorescent foci to appear (ENs, Fig. 2, red foci) are associated with short chromosome core segments (Fig. 2A, green cores) and phosphorylated histone H2AX domains (Fig. 2A, red chromatin) that are indicative of DNA breaks (Fernandez-Capetillo et al., 2004). The developmental progression from zero to 250+ foci during leptotene (Moens et al., 2002) places the nucleus in Fig. 2A, which has 100 foci, at an early leptotene stage. The excess of core segments over RAD51-DMC1 foci indicates that core formation precedes the development of ENs. That RAD51-DMC1 foci are preferentially associated with core segments suggests that EN development may have a functional interaction with core components. If spermatocyte cores are the fusion product of short initial core segments (Fig. 2A), it would limit the number of ENs per core to the available initial segments. These ENs have a fairly even distribution along the cores (ν=2.97, supplementary material Fig. S1A,B). When we simulate synapsis between such cores, the gamma shape is reduced to ν=1.65 (supplementary material Fig. S1C,D). In other words, there is a loss in regulated spacing of foci. However, no such loss is observed along the completed SC at early pachytene (supplementary material Figs S2, S3; ν is ~4). Reduction of ENs at this time may be regulated to restore an even distribution after synapsis.

For the establishment of ENs, there is no absolute requirement either for γH2AX chromatin (supplementary material, Fig. S4), for the recombinase DMC1 (Pittman et al., 1998), the mismatch repair homolog MSH4 (Kneitz et al., 2000), or for the core component SYCP3 (Wang and Hoog, 2006). However, in the cases where these components are disrupted, the numbers, distribution, or turnover of ENs may be affected. Core cohesin protein SMC3, ENs and γH2AX chromatin are exclusively colocated in the restricted synaptic segments of chromosome cores in *Stethophyma grossum* spermatocytes (Calvente et al., 2005). A requirement for SMC1, STAG3 or REC8 in the establishment of ENs has not been reported.

Numbers of ENs decline while cells are still in the leptotene stage (Fig. 2C has 210 foci) and by the time the cores are full length, the fewer ENs are fairly evenly spaced along the unpaired cores (Fig. 2D,E; supplementary material Fig. S1). H2AX-null spermatocytes have fewer foci than wild type but the foci are reasonably well spaced (supplementary material Fig. S4). This can be interpreted to mean that γH2AX is not a major factor for generating ENs (Celeste et al., 2002; Celeste et al., 2003) or for generating an even distribution. The role of γH2AX in DNA-damage detection and repair (Fernandez-Capetillo et al., 2004) led us to expect more pronounced effects in γH2AX-null spermatocytes. Possibly losses of defective prophase spermatocytes confound the tally of EN numbers and positions.

Crossover-non-crossover differentiation

The SC has been invoked as the supra molecular structure to explain the interference pattern of crossovers that are separated at the molecular level by mega up to giga numbers of bases (reviewed by Roeder, 1997). Holliday (Holliday, 1977) proposed that a limited supply of DNA-binding protein required for stabilization of a crossover is located within the SC where it is depleted at the site of, and in the vicinity of, a crossover. King and Mortimer (King and Mortimer, 1990) suggest that ENs bind randomly to the SC and that central-element-associated polymerization reactions prevent additional ENs from binding to the SC or eject ENs that have not started a polymerization reaction. ENs that initiate polymerization reactions are thought to become the recombination nodules. Egel (Egel, 1978; Egel, 1995) echoes this concept: “Positive crossover interference is attributed to the prevention of crossing-over by the growing synaptonemal complex”. Egel (Egel, 1995) based his arguments, among other things, on the evidence that interference is lacking in *Schizosaccharomyces*

pombe and *Apergillus nidulans* that have reciprocal recombination but no SCs. He concludes that the central region of the SC is required for the mediation of crossover interference. Our observation can provide a physical basis for these conjectures.

Recent evidence from *Arabidopsis* and yeast meiosis has generated considerations of mechanisms where the regulation of crossing over is independent of the synaptonemal complex. Cytogenetic analysis of central element transverse filament protein ZYP1-deficient *Arabidopsis* led Higgins et al. (Higgins et al., 2005) and Osman et al. (Osman et al., 2006) to conclude that SC formation is not required for the imposition of crossover interference. These observations, and those of meiotic mutants in *Saccharomyces cerevisiae*, indicate that the crossover-non-crossover decision is made prior to SC formation (Storlazzi et al., 1996; Fung et al., 2004; Börner et al., 2004; Bishop and Zickler, 2004). Several of our observations can also be interpreted in terms of early functional differentiation. We show that in the mouse at the leptotene-to-zygotene transition, the chromosome cores are fully formed and they are mostly aligned while synapsis is still limited (Fig. 3). At this time, it is evident that some of the RPA-TNs form interhomolog structural connections before SC formation. Slightly later, the RPA-TNs are at the synaptic forks of SC progression (Fig. 4). The two types of interhomolog contacts, without and with SCs, could create two classes of interactions (Anderson et al., 2001; Brown et al., 2005). Given that MLH1-containing recombination complexes, RNs, are the sites of chiasmata (crossovers) (Baker et al., 1996; Froenicke et al., 2002; Marcon and Moens, 2003), the MLH1-defined RNs in SC-defective *Sycp3*$^{-/-}$ oocytes (Fig. 6) (Wang and Hoog, 2006) indicate that TNs can acquire MLH1 protein independently of an SC-like structure. Thus, it is feasible that initial-contact TNs without SCs (Fig. 2) are the TNs that are destined to become RNs in mutant and wild-type spermatocytes. That initial contact is the source of SC formations and crossing over has been reported for crossing over and SC formation in an inversion loop in maize (Maguire and Reiss, 1994).

Because there is a tenfold excess of TNs over RNs, most of the TNs are eliminated from the crossover pathway. Few of the proximal TNs and none of the unpaired X chromosome-associated TNs will give rise to reciprocal recombinants. At this level of discrimination, it is apparent that numerous TNs are predestined to be non-crossovers at early meiotic prophase.

At early pachytene when synapsis is just completed, TNs are more evenly spaced than would be expected from a random placement along the SCs as calculated by the gamma distribution (de Boer, 2006) (supplementary material Figs S2, S3: cells 08 and 02). As TNs are lost, spacing takes on a more random distribution (supplementary material Fig. S5, cell 09; Fig. 5B; Table 2). Apparently, the removal of TNs (Fig. 5B, Fig. 7) does not follow a systematic pattern that preserves the even distribution of TNs in early prophase.

γH2AX at meiotic prophase

Mouse ENs contain recombinases RAD51 and DMC1 and they are associated with the sites of programmed double-strand DNA breaks where they function in homology search and strand exchange (reviewed by Bannister and Schimenti, 2004; Page and Hawley, 2004). Whole-mount spreads of early leptotene stages show that the modified chromatin domains are centred around ENs, and spaces between well-separated ENs do not have γH2AX (Fig. 2). It is, therefore, likely that the DSBs at the ENs are the source of chromatin modification.

Considering the large size of the γH2AX domains, it might be possible that the domain would prevent an additional DSB nearby and thereby be a factor in the regulation of DSB spacing. To test that hypothesis, the inter-TN distances were measured in spermatocytes deficient for histone H2AX (supplementary material Fig. S4). It appears that the distribution of 140 TNs is relatively even (gamma shape 2.3) and no case can be made for a strong effect of H2AX absence on TN distribution.

Bouquet et al. (Bouquet et al., 2006) reported that DSB repair is coincident with the disappearance of the γH2AX signal after ionizing radiation was used to induce low levels of DSBs in DNA repair-proficient cells. Dephosphorylation of γH2AX by protein phosphatase 2A is required for DSB repair (Chowdhury et al., 2005). We observe that the loss of extensive γH2AX domains is coincident with synapsis (Fig. 2D,E, Fig. 8A). It can be seen that the TNs along the unpaired cores are associated with γH2AX domains whereas the TNs of nearby chromosomes that have completed synapsis have little or no γH2AX chromatin. Therefore, it seems probable that the components of the ENs (RAD51-DMC1) and TNs (BLM-RPA-MSH4-topoisomerase) have acted so that the SPO11-induced breaks are concealed by repair or joint molecule formation at the zygotene-to-pachytene transition.

A different class of γH2AX domains develops in association with transcriptional silencing of X-Y chromatin at mid to late pachytene (Fig. 8B-D) (Fernandez-Capetillo et al., 2003; Turner et al., 2005). The γH2AX domains are associated with ATR (ataxia telangiectasia- and RAD3-related) and TOPBP1 (topoisomerase binding protein) chromatin of unpaired X and Y cores and with cores of autosomes that have failed to complete synapsis at mid to late pachytene (Fig. 8C) (Moens et al., 1999; Perera et al., 2004). Since γH2AX domains decline at zygotene, we consider the possibility that large domains at mid to late pachytene represent silenced chromatin not only of the X-Y chromatin and the laggards, but also of silenced autosomal loci (Fig. 8B). If indeed silencing of autosomal foci occurs, then γH2AX domains at mid to late pachytene should be in matched pairs. To visualize the positions of γH2AX domains along the pachytene bivalents, we treated spermatocytes with the phosphatase inhibitor okadaic acid that prematurely separates homologs (Fig. 8D) (Cobb et al., 1999; Tarsounas et al., 1999; Marcon and Moens, 2003). It was possible to detect a number of matched γH2AX domains that might support the concept of autosomal silencing. The high density of γH2AX domains in Fig. 8D is the result of inhibition of dephosphorylation of EN- and TN-associated γH2AX domains.

Do TNs become RNs?

A third type of SC-associated nodule is the electron-dense recombination nodules (RN) (Fig. 7B,C) that appears at late prophase in low numbers – one or two per mouse spermatocyte SC. The correlation between RNs and genetic recombination was established in *Drosophila* by Carpenter (Carpenter, 1975; Carpenter, 1979a; Carpenter, 1979b) and confirmed in the mouse by Anderson et al. (Anderson et al., 1999) and by Froenicke et al. (Froenicke et al., 2002). RNs are

imunocytologically detected by the presence of MLH1 protein foci, a homolog of *E. coli* DNA-repair MutL protein (Fig. 7B,C) (Baker et al., 1996; Froenicke et al., 2002). RN/MLH1 foci were shown to be associated with chiasmata in mouse spermatocytes (Fig. 7D inset) (Marcon and Moens, 2003).

There is uncertainty about the origin of RNs. Do they originate independently of TNs or are they derived from a subset of TNs and, if so, which subset? We assume that protein composition of TNs and RNs can provide evidence for structural continuity from TN to RN. Relative amounts of different antigens can be resolved accurately by immunoelectron microscopy through quantitative assessment of gold grains. We observe that in nuclei where RNs are starting to develop (Fig. 7E), the RNs contain both RPA and MLH1 antigen (Fig. 7B,C) supporting the concept that RNs develop from TNs. The resolution of immunogold further distinguishes the precise localization of foci relative to SC components, central element and lateral elements.

Are most TNs resolved as non-crossovers?

Following the induction of programmed DNA double-strand breaks and resection (Bishop and Zickler, 2004), the single-strand overhangs become associated with RAD51/DMC1 protein complexes that function in homology search and strand exchange. Eventually, the ENs/TNs mark the sites of joint molecules (see Page and Hawley, 2004). Resolution of these joint molecules requires DNA synthesis to fill in the gaps from DSB induction and resection (Gilbertson and Stahl, 1996). If the repair synthesis can be detected, one would expect there to be several such sites along each autosomal SC. In vitro exposure of mouse pachytene spermatocytes to 1 hour of [^{3}H]thymidine results in several groups of silver grains along each autosomal SCs and one group at the PAR region of the X-Y cores (Moses et al., 1984). Because most of the SCs have only one crossover, the majority of the joint molecules that have undergone repair synthesis and possibly gene conversion seem to be resolved as non-crossovers.

Resolution of joint molecules as non-crossovers can be accomplished either by movement of the Holliday junction into unligated strands or by the concerted action of helicases and topoisomerases (Gibertson and Stahl, 1996; Plank et al., 2006).

At the cytological level, we observe that, at late prophase, the TNs are displaced from the medial region of the SCs to the outside of the lateral elements (Fig. 7B,C). One possible interpretation is that the lateral displacement induces directional stress-activated activity of the topoisomerase-resolving joint molecules that are associated with the TNs.

Materials and Methods

Spermatocytes for immunocytology were obtained from adult wild-type CD-1 mice and *Sycp3*$^{-/-}$ mice (Yuan et al., 2000) kindly donated by C. Hoog, Karolinska Institute, Sweden, and H2AX-null mice that were kindly given to us by A. Nussenzweig, NIH [characterized by Celeste et al. (Celeste et al., 2002)]. We used antibodies raised in rabbits and mice against hamster 30 kDa chromosome core protein, COR1 and 110 kDa central-element transverse filaments, SYN1 (Dobson et al., 1994), named thus to differentiate it from the rat SC components SCP3 and SCP1 (Heyting et al., 1987). The designations COR1 and SYN1 are widely used by investigators who use our antibodies. Later, the 30-33 kDa cores were renamed SYCP3 and transverse filaments SYCP1 (Sage et al., 1999; Botelho et al., 2001), and for conformity we use the terminology anti-SYCP3 and anti-SYCP1 for our anti-COR1 and anti-SYN1 antibodies.

Spermatocytes were prepared for fluorescence or electron microscope immunocytology as reported previously (Dobson et al., 1994). Chromosome cores and synaptonemal complexes were visualized with hamster anti-SYCP3 and anti-SYCP1. SC- and core-associated proteins that are involved in recombination processes were visualized with antibodies to trimeric RPA (replication protein A) (He et al., 1995), MLH1 (MutL homolog; Pharmingen) and cohesins SMC3 and STAG 3 (a gift from R. Jessberger, Dresden, Germany). Our treatment of short-term spermatocyte cultures with the phosphatase inhibitor, okadaic acid, was reported previously (Marcon and Moens, 2003). The distribution of ENs/TNs was measured by distances between fluorescent ENs and TNs or recorded on electron micrographs of full-length SCs with immunogold TNs. We used the method of maximum likelihood to fit the gamma distribution to the observed interfocus distance (μm) data for SCs of cells at various stages of prophase I. We also did the analyses using data that were standardized so that the length of each SC was first scaled to 100. The shape (ν) and rate (λ) parameters of the gamma distribution were both estimated as were their standard errors and/or their 95% confidence intervals. We also conducted the estimation of rate (λ) assuming the shape ν=1.0 (implying no interference) (de Boer, 2006) and conducted a log likelihood ratio test (using the G-statistic with 1 degree of freedom) (Zar, 1999) to determine whether ν differed significantly from 1.0. Maximum likelihood estimation was performed using the R statistical programming language (R Development Core Team, 2004; Ricci, 2005). We also assessed the goodness of fit (using the χ^2 goodness of fit statistic) of the gamma distribution by binning the observed data into a number of distance classes, and calculated the expected frequencies obtained from the gamma distribution, given the maximum likelihood estimates of the shape and rate parameters. We pooled the larger-distance classes when the expected numbers were less than approximately five. The degrees of freedom were calculated as the number of classes minus three (as two parameters were estimated from the data).

Financial assistance was provided by a Natural Sciences and Engineering Research Council of Canada Discovery Grant to P.B.M. and a Graduate Scholarship to E.M.

References

Anderson, L. K., Offenberg, H. H., Verkuijlen, W. M. and Heyting, C. (1997). RecA-like proteins are components of early meiotic nodules in lily. *Proc. Natl. Acad. Sci. USA* **94**, 6868-6873.

Anderson, L. K., Reeves, A., Webb, L. M. and Ashley, T. (1999). Distribution of crossing over on mouse synaptonemal complexes using immunofluorescent localization of MLH1 protein. *Genetics* **151**, 1569-1579.

Anderson, L. K., Hooker, K. D. and Stack, S. M. (2001). The distribution of early recombination nodules on zygotene bivalents from plants. *Genetics* **159**, 1259-1269.

Ashley, T., Plug, A. W., Xu, J., Solari, A. J., Reddy, G., Golub, E. I. and Ward, D. C. (1995). Dynamic changes in Rad51 distribution on chromatin during meiosis in male and female vertebrates. *Chromosoma* **104**, 19-28.

Baker, S. M., Plug, A. W., Prolla, T. A., Bronner, C. E., Harris, A. C., Yao, X., Christie, D. M., Monell, C., Arnheim, N., Bradley, A. et al. (1996). Involvement of mouse Mlh1 in DNA mismatch repair and meiotic crossing over. *Nat. Genet.* **13**, 336-342.

Bannister, L. A. and Schimenti, J. C. (2004). Homologous recombinational repair proteins in mouse meiosis. *Cytogenet. Genome Res.* **107**, 191-200.

Bishop, D. K. (1994). RecA homologs Dmc1 and Rad51 interact to form multiple nuclear complexes prior to meiotic chromosome synapsis. *Cell* **79**, 1081-1092.

Bishop, D. K. and Zickler, D. (2004). Early decision; meiotic crossover interference prior to stable strand exchange and synapsis. *Cell* **117**, 9-15.

Blat, Y., Protacio, R. U., Hunter, N. and Kleckner, N. (2002). Physical and functional interactions among basic chromosome organizational features govern early steps of meiotic chiasma formation. *Cell* **111**, 791-802.

Börner, G. V., Kleckner, N. and Hunter, N. (2004). Crossover/noncrossover differentiation, synaptonemal complex formation, and regulatory surveillance at the leptotene/zygotene transition of meiosis. *Cell* **117**, 29-45.

Botelho, R. J., DiNicolo, L., Tsao, N., Karaiskakis, A., Tarsounas, M., Moens, P. B. and Pearlman, R. E. (2001). The genomic structure of SYCP3, a meiosis-specific gene encoding a protein of the chromosome core. *Biochim. Biophys. Acta* **1518**, 294-299.

Bouquet, F., Muller, C. and Salles, B. (2006). The loss of gammaH2AX signal is a marker of DNA double strand breaks repair only at low levels of DNA damage. *Cell Cycle* **5**, 1116-1122.

Brown, P. W., Judis, L., Chan, E. R., Schwartz, S., Seftel, A., Thomas, A. and Hassold, T. J. (2005). Meiotic synapsis proceeds from a limited number of subtelomeric sites in the human male. *Am. J. Hum. Genet.* **77**, 556-566.

Calvente, A., Viera, A., Page, J., Parra, M. T., Gomez, R., Suja, J. A., Rufas, J. S. and Santos, J. L. (2005). DNA double-strand breaks and homology search: inferences from a species with incomplete pairing and synapsis. *J. Cell Sci.* **118**, 2957-2963.

Carpenter, A. T. C. (1975). Electron microscopy of meiosis in *Drosophila melanogaster* females: I. The recombination nodule: a recombination-associated structure at pachytene? *Proc. Natl. Acad. Sci. USA* **72**, 3186-3189.

Carpenter, A. T. C. (1979a). Synaptonemal complex and recombination nodules in wild-type *Drosophila melanogaster* females. *Genetics* **92**, 511-541.

Carpenter, A. T. C. (1979b). Synaptonemal complex and recombination nodules in recombination-deficient mutants of *Drosophila melanogaster*. *Chromosoma* **75**, 259-292.

Celeste, A., Petersen, S., Romanienko, P. J., Fernandez-Capetillo, O., Chen, H. T.,

Sedelnikova, O. A., Reina-San-Martin, B., Coppola, V., Meffre, E., Difilippantonio, M. J. et al. (2002). Genomic instability in mice lacking histone H2AX. *Science* **296**, 922-927.
Celeste, A., Fernandez-Capetillo, O., Kruhlak, M. J., Pilch, D. R., Staudt, D. W., Lee, A., Bonner, R. F., Bonner, W. M. and Nussenzweig, A. (2003). Histone H2AX phosphorylation is dispensable for the initial recognition of DNA breaks. *Nat. Cell Biol.* **5**, 675-679.
Chowdhury, D., Keogh, M. C., Ishii, H., Peterson, C. L., Buratowski, S. and Lieberman, J. (2005). Gamma-H2AX dephosphorylation by protein phosphatase 2A facilitates DNA double-strand break repair. *Mol. Cell* **20**, 801-809.
Cobb, J., Cargile, B. and Handel, M. A. (1999). Acquisition of competence to condense metaphase I chromosomes during spermatogenesis. *Dev. Biol.* **205**, 49-64.
de Boer, E., Stam, P., Dietrich, A. J., Pastink, A. and Heyting, C. (2006). Two levels of interference in mouse meiotic recombination. *Proc. Natl. Acad. Sci. USA* **103**, 9607-9612.
Dobson, M. J., Pearlman, R. E., Karaiskakis, A., Spyropoulos, B. and Moens, P. B. (1994). Synaptonemal complex proteins: occurrence, epitope mapping and chromosome disjunction. *J. Cell Sci.* **107**, 2749-2760.
Egel, R. (1978). Synaptonemal complex and crossing-over: structural support or interference? *Heredity* **41**, 233-237.
Egel, R. (1995). The synaptonemal complex and the distribution of meiotic recombination events. *Trends Genet.* **11**, 206-208.
Fernandez-Capetillo, O., Mahadevaiah, S. K., Celeste, A., Romanienko, P. J., Camerini-Otero, R. D., Bonner, W. M., Manova, K., Burgoyne, P. and Nussenzweig, A. (2003). H2AX is required for chromatin remodeling and inactivation of sex chromosomes in male mouse meiosis. *Dev. Cell* **4**, 497-508.
Fernandez-Capetillo, O., Lee, A., Nussenzweig, M. and Nussenzweig, A. (2004). H2AX: the histone guardian of the genome. *DNA Repair Amst.* **3**, 959-967.
Froenicke, L., Anderson, L. K., Wienberg, J. and Ashley, T. (2002). Male mouse recombination maps for each autosome identified by chromosome painting. *Am. J. Hum. Genet.* **71**, 1353-1368.
Fung, J. C., Rockmill, B., Odell, M. and Roeder, G. S. (2004). Imposition of crossover interference through the nonrandom distribution of synapsis initiation complexes. *Cell* **16**, 795-802.
Gilbertson, L. A. and Stahl, F. W. (1996). A test of the double-strand break repair model for meiotic recombination in *Saccharomyces cerevisiae*. *Genetics* **144**, 27-41.
He, Z., Henricksen, L. A., Wold, M. S. and Ingles, C. J. (1995). RPA involvement in the damage-recognition and incision steps of nucleotide excision repair. *Nature* **374**, 566-569.
Heyting, C., Moens, P. B., van Raamsdonk, W., Dietrich, A. J., Vink, A. C. and Redeker, E. J. (1987). Identification of two major components of the lateral elements of synaptonemal complexes of the rat. *Eur. J. Cell Biol.* **43**, 148-154.
Higgins, J. D., Sanchez-Moran, E., Armstrong, S. J., Jones, G. H. and Franklin, F. C. H. (2005). The *Arabidopsis* synaptonemal complex protein ZYP1 is required for chromosome synapsis and normal fidelity of crossing over. *Genes Dev.* **19**, 2488-2500.
Holliday, R. (1977). Recombination and meiosis. *Philos. Trans. R. Soc. Lond. B Biol. Sci.* **277**, 359-370.
Jones, G. H. (1984). The control of chiasma distribution. *Symp. Soc. Exp. Biol.* **38**, 293-320.
Jones, G. H. (1987). Chiasmata. In *Meiosis* (ed. P. B. Moens), pp. 213-244. New York: Academic Press.
King, J. S. and Mortimer, R. K. (1990). A polymerization model of chiasma interference and corresponding computer simulation. *Genetics* **126**, 1127-1138.
Kneitz, B., Cohen, P. E., Avdievich, E., Zhu, L., Kane, M. F., Hou, H., Jr, Kolodner, R. D., Kucherlapati, R., Pollard, J. W. and Edelmannm, W. (2000). MutS homolog 4 localization to meiotic chromosomes is required for chromosome pairing during meiosis in male and female mice. *Genes Dev.* **14**, 1085-1097.
Kolas, N. K., Marcon, E., Crackower, M. A., Hoog, C., Penninger, J. M., Spyropoulos, B. and Moens, P. B. (2005). Mutant meiotic chromosome core components in mice can cause apparent sexual dimorphic endpoints at prophase or X-Y defective male-specific sterility. *Chromosoma* **114**, 92-102.
Maguire, M. P. and Reiss, R. W. (1994). The relationship of homologous synapsis and crossing over in a maize inversion. *Genetics* **137**, 281-288.
Marcon, E. and Moens, P. (2003). MLH1p and MLH3p localize to precociously induced chiasmata of okadaic-acid-treated mouse spermatocytes. *Genetics* **165**, 2283-2287.
Moens, P. B., Chen, D. J., Shen, Z., Kolas, N., Tarsounas, M., Heng, H. H. and Spyropoulos, B. (1997). Rad51 immunocytology in rat and mouse spermatocytes and oocytes. *Chromosoma* **106**, 207-215.
Moens, P. B., Tarsounas, M., Morita, T., Habu, T., Rottinghaus, S. T., Freire, R., Jackson, S. P., Barlow, C. and Wynshaw-Boris, A. (1999). The association of ATR protein with mouse meiotic chromosome cores. *Chromosoma* **108**, 95-102.
Moens, P. B., Kolas, N. K., Tarsounas, M., Marcon, E., Cohen, P. E. and Spyropoulos, B. (2002). The time course and chromosomal localization of recombination-related proteins at meiosis in the mouse are compatible with models that can resolve the early DNA-DNA interactions without reciprocal recombination. *J. Cell Sci.* **115**, 1611-1622.
Moses, M. J., Dresser, M. E. and Poorman, P. A. (1984). Composition and role of the synaptonemal complex. *Symp. Soc. Exp. Biol.* **38**, 245-270.
Osman, K., Sanchez-Moran, E., Higgins, J. D., Jones, G. H. and Franklin, F. C. (2006). Chromosome synapsis in *Arabidopsis*: analysis of the transverse filament protein ZYP1 reveals novel functions for the synaptonemal complex. *Chromosoma* **115**, 212-219.
Page, S. L. and Hawley, R. S. (2004). The genetics and molecular biology of the synaptonemal complex. *Annu. Rev. Cell Dev. Biol.* **20**, 525-528.
Perera, D., Perez-Hidalgo, L., Moens, P. B., Reini, K., Lakin, N., Syvaoja, J. E., San-Segundo, P. A. and Freire, R. (2004). TopBP1 and ATR colocalization at meiotic chromosomes: role of TopBP1/Cut5 in the meiotic recombination checkpoint. *Mol. Biol. Cell* **15**, 1568-1579.
Pittman, D. L., Cobb, J., Schimenti, K. J., Wilson, L. A., Cooper, D. M., Brignull, E., Handel, M. A. and Schimenti, J. C. (1998). Meiotic prophase arrest with failure of chromosome synapsis in mice deficient for Dmc1, a germline-specific RecA homolog. *Mol. Cell* **1**, 697-705.
Plank, J. L., Wu, J. and Hsieh, T. S. (2006). Topoisomerase IIIα and Bloom's helicase can resolve a mobile double Holliday junction substrate through convergent branch migration. *Proc. Natl. Acad. Sci. USA* **103**, 11118-11123.
R Development Core Team (2004). *R: A Language and Environment for Statistical Computing*. Vienna, Austria: R Foundation for Statistical Computing.
Revenkova, E. and Jessberger, R. (2005). Keeping sister chromatids together: cohesins in meiosis. *Reproduction* **130**, 783-790.
Ricci, V. (2005). *Fitting Distributions with R*. Vienna, Austria: R Foundation for Statistical Computing.
Roeder, G. S. (1997). Meiotic chromosomes: it takes two to tango. *Genes Dev.* **11**, 2600-2621.
Sage, J., Martin, L., Meuwissen, R., Heyting, C., Cuzin, F. and Rassoulzadegan, M. (1999). Temporal and spatial control of the Sycp1 gene transcription in the mouse meiosis: regulatory elements active in the male are not sufficient for expression in the female gonad. *Mech. Dev.* **80**, 29-39.
Shinohara, M., Gasior, S. L., Bishop, D. K. and Shinohara, A. (2000). Tid1/Rdh54 promotes colocalization of rad51 and dmc1 during meiotic recombination. *Proc. Natl. Acad. Sci. USA* **97**, 10814-10819.
Storlazzi, A., Xu, L., Schwacha, A. and Kleckner, N. (1996). Synaptonemal complex (SC) component Zip1 plays a role in meiotic recombination independent of SC polymerization along the chromosomes. *Proc. Natl. Acad. Sci. USA* **93**, 9043-9048.
Tarsounas, M., Morita, T., Pearlman, R. E. and Moens, P. B. (1999). RAD51 and DMC1 form mixed complexes associated with mouse meiotic chromosome cores and synaptonemal complexes. *J. Cell Biol.* **147**, 207-220.
Turner, J. M., Mahadevaiah, S. K., Fernandez-Capetillo, O., Nussenzweig, A., Xu, X., Deng, C. X. and Burgoyne, P. S. (2005). Silencing of unsynapsed meiotic chromosomes in the mouse. *Nat. Genet.* **37**, 41-47.
Wang, H. and Hoog, C. (2006). Structural damage to meiotic chromosomes impairs DNA recombination and checkpoint control in mammalian oocytes. *J. Cell Biol.* **173**, 485-495.
Yuan, L., Liu, J. G., Zhao, J., Brundell, E., Daneholt, B. and Hoog, C. (2000). The murine SCP3 gene is required for synaptonemal complex assembly, chromosome synapsis, and male fertility. *Mol. Cell* **5**, 73-83.
Zar, J. H. (1999). *Biostatistical Analysis*. Upper Saddle River, NJ: Prentice-Hall.

Journal of Cell Science